ChemComm

COMMUNICATION

View Article Online
View Journal | View Issue

An MnO_2 nanosheet as a label-free nanoplatform for homogeneous biosensing†

Cite this: *Chem. Commun.*, 2014, **50**, 1095

Received 9th October 2013,
Accepted 19th November 2013

DOI: 10.1039/c3cc47755j

www.rsc.org/chemcomm

Yunxia Yuan, Shufang Wu, Fan Shu and Zhihong Liu*

An ultrathin MnO_2 nanosheet is established as a label-free two-dimensional nanoplatform for homogeneous biosensing. Two biosensors based on an MnO_2 nanosheet with favourable performances are constructed for OTA and Cat D using different probes and following different sensing principles.

Two-dimensional (2D) nanomaterials with light harvesting and/or electron-conduction abilities have emerged as promising nanoplatforms for bio-/chemo-sensing, based on the mechanisms of fluorescence resonance energy transfer (FRET), photo-induced electron transfer (PET) and so on.[1] The 2D materials possess planar structure and ultra-large surface areas which enable easy wiring with biomolecules. Besides, they also provide excellent sensing performances due to the good light absorption and electron-transfer rate. Graphitic carbon materials (graphene or graphene oxide) are the most famous representatives that have gained successful applications, with which the probe molecules are generally assembled *via* π–π stacking and hydrophobic interactions.[2] A single-layer MoS_2 nanosheet is another 2D material with its structure analogous to graphene, which was lately reported as an energy acceptor in homogenous FRET sensing.[3] Manganese dioxide (MnO_2) nanosheets have drawn increasing attention in recent years and found applications in lithium batteries, supercapacitors and so forth.[4] An MnO_2 nanosheet consisting of an edge-shared MnO_6 octahedral crystal lattice has the thickness on the order of nanometers or smaller with lateral size ranging from submicrometers to micrometers. As a result of the d–d transition of Mn ions in the ligand field of MnO_6 octahedra, MnO_2 has intense and broad light absorption.[5,6] Most recently, Liu *et al.* revealed that the fluorescence emission of luminescent nanoparticles was quenched by MnO_2 when they coated MnO_2 on the surface of the nanoparticles.[7] Inspired by the above knowledge and findings, we expect that MnO_2 nanosheets could be another potential label-free nanoplatform for homogeneous biosensing with wide applications.

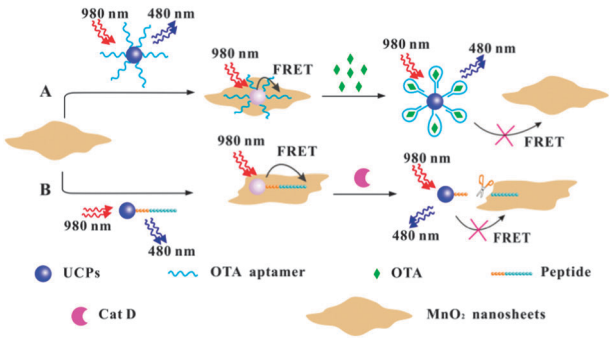

Scheme 1 Schematic illustration (not to real scale) of MnO_2 nanosheet-based FRET sensing. (A) The OTA sensor with an ssDNA as the probe; (B) the Cat D sensor with a peptide as the probe.

We herein propose a homogeneous FRET sensing protocol using an MnO_2 nanosheet as the energy acceptor for the first time, which makes use of the light absorption of MnO_2. At an initial trial, we use an ssDNA chain as the probe and ochratoxin A (OTA) as the sensing target. As shown in Scheme 1A, the OTA aptamers tagged to fluorophores are spontaneously assembled on the flat surface, resulting in the energy transfer from the fluorophore to MnO_2 and the quenching of the fluorescence. The interaction of the aptamers with OTA molecules changes the conformation of the aptamers, which reduces the exposure of the nucleobases. As a consequence, the physisorption of the aptamers on MnO_2 surface is weakened. In this situation, the emission of the fluorophore is expected to be recovered, which enables the recognition and quantification of the target.

To realize the above design, we firstly synthesized the MnO_2 nanosheet according to a reported procedure with modifications (see ESI† for details).[8] The TEM image of the product (Fig. S1a, ESI†) revealed a large 2D and ultrathin plane with occasional folds and wrinkles. Energy dispersive spectroscopy (EDS) analysis (Fig. S1b, ESI†) indicated the presence of Mn and O elements. The absorption spectrum exhibited a wide band in the range of 230–700 nm with a peak located at 378 nm (Fig. S1c, ESI†), which is the characteristic

Key Laboratory of Analytical Chemistry for Biology and Medicine (Ministry of Education), College of Chemistry and Molecular Sciences, Wuhan University, Wuhan 430072, P. R. China. E-mail: zhhliu@whu.edu.cn; Fax: +86 27-6875-4067

† Electronic supplementary information (ESI) available: Materials, experimental details, characterization data, control experiments and fluorescence quenching in red wine and human serum samples. See DOI: 10.1039/c3cc47755j

absorption for the MnO_2 sheet.[5–8] The broad absorption will make the energy acceptor adaptable to diverse fluorophores emitting at different regions. The absorbance was observed to be linearly dependent on the concentration of MnO_2 (Fig. S1d, ESI†). In this work, we selected Tm-doped upconversion phosphors (UCPs), $NaYF_4$:Yb, Tm, as the energy donors. The reason for using this kind of energy donor was to examine the applicability of the MnO_2 nanosheet in complicated sample matrixes, which is important for its practical use. Because UCPs are known for their ability to eliminate background noises in optical sensing in complicated samples owing to their NIR-excitation nature,[9,10] the possible excitation-related interference can be precluded. Water-soluble polyacrylic acid (PAA) modified $NaYF_4$:Yb, Tm nanoparticles with an average size of ~50 nm and cubic phase (Fig. S2, ESI†) were prepared using our established route.[9,10] The OTA aptamer was linked to the carboxyl groups on UCPs using the EDC–NHS coupling strategy. The successful conjugation was confirmed by UV-Vis spectra (Fig. S3, ESI†).

Upon the incubation of the UCPs–aptamer complex with the MnO_2 nanosheet, the aptamers were adsorbed on the surface of the nanosheet. Consequently, the fluorescence emission of UCPs was efficiently quenched (Fig. 1a), which was due to the resonance energy transfer from UCPs to the dark quencher. A control experiment showed that the fluorescence quenching degrees of bare UCPs (without linking aptamers) using a MnO_2 nanosheet were much lower than that of UCPs–aptamer complexes (Fig. S4, ESI†), indicating the occurrence of spontaneous assembly of the ssDNA chains on the nanosheet, which can be evidenced by comparing the FT-IR spectra before and after the assembly (Fig. S5, ESI†). The assembly is assigned mainly to van der Waals forces between nucleobases and the nanosheet. Unlike the 2D graphitic materials possessing a large electronic conjugate system, the MnO_2 nanosheet does not afford π–π stacking with the nucleobases. On the other hand, electrostatic interaction between the negatively charged DNA chains and the MnO_2 nanosheet is excluded since the latter was also negatively charged, as shown using the zeta potential of −58.5 mV (Fig. S6, ESI†). In another control experiment, we linked dsDNA chains to the UCPs and found that the quenching of the fluorescence of UCPs–dsDNA complex by MnO_2 was remarkably lower than that of UCPs–ssDNA (Fig. S7, ESI†). This is explained using the fact that the hybridized base pairs in the dsDNA chain are shielded by the phosphate backbone, which reduces the van der Waals force and inhibits the physisorption of the dsDNA chain on the nanosheet. This result also suggested the feasibility of using the MnO_2 nanoplatform to construct DNA hybridization-based sensors in the future. In the UCPs–MnO_2 FRET pair, the fluorescence quenching degree was dependent on the concentration of MnO_2 nanosheet and a maximum quenching degree of up to 90% was achieved using the 0.5 mg mL^{-1} quencher (Fig. 1b). The plateau on the quenching curve (Fig. 1b) ensures stable quenching in subsequent assays. Besides, the time dependence of the quenching (Fig. 1c) shows that the interaction of aptamers with the nanosheet reached equilibrium very quickly (in only a few minutes), which is also in favour of practical applications.

We then investigated the performance of this FRET system for homogeneous OTA sensing, firstly in an aqueous buffer. With the addition of free OTA to the solution containing the UCPs–aptamer complex and MnO_2 nanosheet, the emission of UCPs was restored in an OTA concentration-dependent manner, as shown in Fig. 2a. It is explained in that the formation of the aptamer–OTA complex decreases the exposure of nucleobases and thus hinders the physisorption of the aptamer on the nanosheet, similar to the situation of the above-mentioned dsDNA chains. The emission of bare UCPs or the UCPs–aptamer was not affected by OTA molecules (data not shown), suggesting that the restoration of UCP emission resulted from the blocking of energy transfer from the UCP to the MnO_2 nanosheet. The relative fluorescence intensity ($(F - F_0)/F_0$, where F and F_0 represent the emission intensity in the presence and in the absence of OTA, respectively) was linearly related to OTA concentration within the range from 0.02 to 2.0 ng mL^{-1}, with a correlation coefficient of 0.994 (Fig. 2b). The quantification limit of this biosensor is as low as 0.02 ng mL^{-1}, which is competitive among reported methods for OTA determination conducted in aqueous solutions.[11] The standard deviations of repeated measurements are at quite low levels, demonstrating a good reproducibility of this MnO_2 nanosheet-based biosensing platform. In order to examine the specificity of the sensor for OTA, the analogues of OTA including aflatoxin B1 (AFB1) and aflatoxin B2 (AFB2) were tested under identical assay conditions. Even with a concentration as high as 200 ng mL^{-1}, which was 100 times higher than that of OTA, AFB1 and AFB2 caused negligible alteration of the UCP emission as compared to OTA (Fig. S8, ESI†).

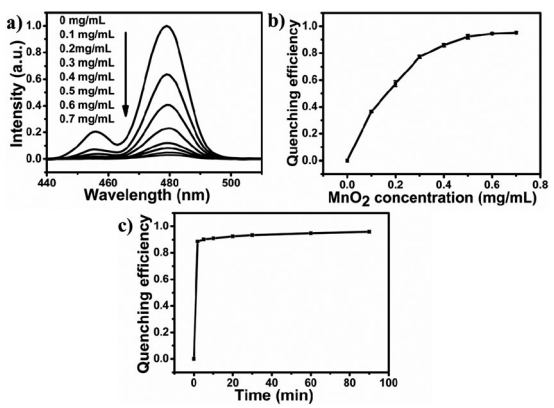

Fig. 1 (a) Fluorescence quenching of the UCPs–aptamer (0.02 mg mL^{-1}) by varying amounts of the MnO_2 nanosheet. (b) Fluorescence quenching degree *versus* MnO_2 nanosheet concentration (0, 0.1, 0.2, 0.3, 0.4, 0.5, 0.6, 0.7 mg mL^{-1}). Data were presented as average ± sd from three independent measurements. (c) Time dependence of the fluorescence quenching with 0.02 mg mL^{-1} UCPs–aptamer and 0.5 mg mL^{-1} MnO_2 nanosheet. Excitation wavelength: 980 nm.

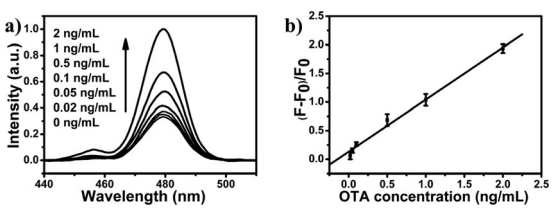

Fig. 2 (a) Fluorescence of the UCPs–aptamer/MnO_2 nanosheet in the presence of different concentrations of OTA (0, 0.02, 0.05, 0.1, 0.5, 1, 2 ng mL^{-1}) in HEPES buffer (pH 7.4, 10 mM, 100 mM NaCl). (b) The linear relationship between the relative fluorescence intensity and the concentration of OTA within the range of 0.02–2 ng mL^{-1}. Data were presented as average ± sd from three independent measurements. Excitation wavelength: 980 nm.

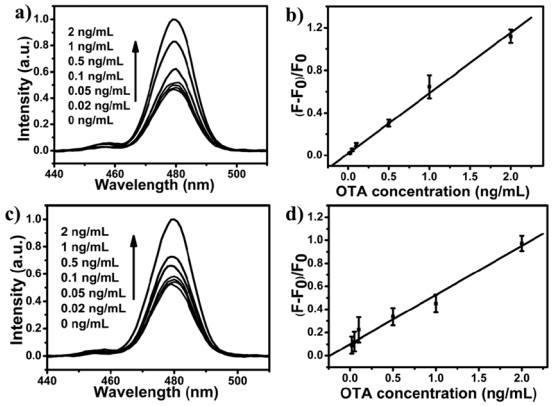

Fig. 3 Fluorescence of the UCPs–aptamer/MnO_2-nanosheet in the presence of different concentrations of OTA (0, 0.02, 0.05, 0.1, 0.5, 1, 2 ng mL^{-1}) in 50-fold diluted red wine (a) and 50-fold diluted human serum (c). The linear relationship between the relative fluorescence intensity and the concentration of OTA within the range of 0.02–2 ng mL^{-1} in diluted red wine (b) and diluted human serum (d). Data were presented as average ± sd from three independent measurements. Excitation wavelength: 980 nm.

Obviously, such a pronounced specificity results from the specific recognition of the target by the aptamer, which again confirms that the change of the aptamer conformation plays a key role in controlling the donor-to-quencher distance and tunes the emission intensity of the donor.

Because of the quite large surface area, such 2D planar materials are likely to be subject to nonspecific adsorption of nontarget species, which might sometimes hinder the target sensing in complicated sample matrixes. Therefore, it is necessary to see whether a linear calibration for the target could still be set up in such samples. To this end, we subsequently conducted the OTA assay in complicated sample matrixes, including a foodstuff sample (red wine purchased from local super market) and a clinical sample (human serum from healthy volunteer). The red wine and human serum samples were 50-fold diluted with buffer solution without further processing. As seen from Fig. S9 and S10 (ESI†), both the efficiency and the kinetics of the fluorescence quenching by the MnO_2 nanosheet in red wine and human serum samples were almost identical to that in aqueous solution, implying that the numerous substances existing in these samples had no obvious influence on either the aptamer assembly or the fluorescence measurement. More significantly, the linear dependence of the restoration of UCP fluorescence on OTA concentration was also obtained in the range of 0.02–2.0 ng mL^{-1} (Fig. 3), the same as in the case of the aqueous solution. The difference is that the slopes of the calibration curves in these two samples were slightly lower than that in buffer solution (Fig. 3b and d), suggesting slightly reduced sensitivities. These results reveal high robustness of the MnO_2 nanosheet-based biosensing in complicated matrixes, which is meaningful and essential for practical applications.

In order to validate the universality of the sensing protocol, we then used a peptide chain as the probe and constructed another FRET sensor for cathepsin D (Cat D), which is based on the specific cleavage of the peptide by Cat D (Scheme 1B). In this case we employed polyethylenimine (PEI) modified $NaYF_4$:Yb, Tm nanoparticles[12] with hexagonal phase and larger size (~100 nm, Fig. S11, ESI†) as the energy donor. A polypeptide chain (see ESI† for sequence) containing six consecutive aromatic amino acids and the Cat D-specific substrate was designed as the probe and linked to the PEI-UCPs (at the C terminus) following the sulfo-SMCC coupling protocol. The successful conjugation was also confirmed by UV-Vis spectra (Fig. S12, ESI†). Similar to the ssDNA probe, the peptide was assembled on the surface of MnO_2 due to the van der Waals interaction between the aromatic residues and the nanosheet, resulting in the quenching of the UCP fluorescence (Fig. S13a and b, ESI†). It is also a quick process that is completed in a few minutes (Fig. S13c, ESI†). With the introduction of Cat D, which specifically cleaves the substrate at the *F–F* site leading to the detachment of UCPs from the MnO_2 nanosheet, the fluorescence intensity of UCPs is gradually restored (Fig. S14a, ESI†). The relative fluorescence intensity at 480 nm was linearly dependent on Cat D concentration within the range of 1–100 ng mL^{-1} (Fig. S14b, ESI†).

In conclusion, we have established a 2D MnO_2 nanosheet as a new label-free nanoplatform for homogeneous biosensing. The nanosheet can be facilely prepared with high dispersibility in water. The sensors constructed on this nanoplatform can be applied in not only aqueous solutions but also complicated sample matrixes with favourable sensing performances, high robustness and easy operations. In addition, the MnO_2 nanoplatform can easily be adapted to other luminescent materials and diverse probes, and therefore wide applications in bio-/chemo-sensing can be expected.

This work was supported by the National Natural Science Foundation of China (No. 21075094, 21375098), the National Basic Research of China (973 program, No. 2011CB933600) and the Program for New Century Excellent Talents in University (NCET-11-0402).

Notes and references

1 Y. Liu, X. Dong and P. Chen, *Chem. Soc. Rev.*, 2012, **41**, 2283; S. Guo and S. Dong, *Chem. Soc. Rev.*, 2011, **40**, 2644.
2 C. H. Lu, H. H. Yang, C. L. Zhu, X. Chen and G. N. Chen, *Angew. Chem., Int. Ed.*, 2009, **48**, 4785; C. Liu, Z. Wang, H. Jia and Z. Li, *Chem. Commun.*, 2011, **47**, 4661.
3 C. Zhu, Z. Zeng, H. Li, F. Li, C. Fan and H. Zhang, *J. Am. Chem. Soc.*, 2013, **135**, 5998.
4 K. Kang, Y. S. Meng, J. Breger, C. P. Grey and G. Ceder, *Science*, 2006, **311**, 977; G. Zhao, J. Li, L. Jiang, H. Dong, X. Wang and W. Hu, *Chem. Sci.*, 2012, **3**, 433.
5 N. Sakai, Y. Ebina, K. Takada and T. Sasaki, *J. Phys. Chem. B*, 2005, **109**, 9651.
6 Y. Omomo, T. Sasaki, L. Z. Wang and M. Watanabe, *J. Am. Chem. Soc.*, 2003, **125**, 3568.
7 R. Deng, X. Xie, M. Vendrell, Y. T. Chang and X. Liu, *J. Am. Chem. Soc.*, 2011, **133**, 20168.
8 K. Kai, Y. Yoshida, H. Kageyama, G. Saito, T. Ishigaki, Y. Furukawa and J. Kawamata, *J. Am. Chem. Soc.*, 2008, **130**, 15938.
9 Y. Wang, L. Bao, Z. Liu and D. W. Pang, *Anal. Chem.*, 2011, **83**, 8130; C. Zhang, Y. Yuan, S. Zhang, Y. Wang and Z. Liu, *Angew. Chem., Int. Ed.*, 2011, **50**, 6851; Y. Wang, P. Shen, C. Li and Z. Liu, *Anal. Chem.*, 2012, **84**, 1466; Y. Wang, Z. Wu and Z. Liu, *Anal. Chem.*, 2013, **85**, 258.
10 Y. Yuan and Z. Liu, *Chem. Commun.*, 2012, **48**, 7510.
11 L. Wang, W. Chen, W. Ma, L. Liu, W. Ma, Y. Zhao, Y. Zhu, L. Xu, H. Kuang and C. Xu, *Chem. Commun.*, 2011, **47**, 1574; S. Wu, N. Duan, X. Ma, Y. Xia, H. Wang, Z. Wang and Q. Zhang, *Anal. Chem.*, 2012, **84**, 6263.
12 F. Wang and X. Liu, *J. Am. Chem. Soc.*, 2008, **130**, 5642.